Solidification of Particle-Reinforced Metal-Matrix Composites

G.S. HANUMANTH and G.A. IRONS

The solidification behavior of ceramic particle-reinforced metal-matrix composites (MMCs) is different from that of the bare matrix, not only because of the presence of the ceramic particles, but also due to their redistribution in the melt that results in nonhomogeneous thermophysical properties. The MMCs comprised of 10- to 15-μm SiC particles of varying volume fractions, dispersed uniformly in a modified aluminum A356 alloy by the melt stirring technique, were solidified unidirectionally in a thermocouple-instrumented cylindrical steel mold. The cooling rates were continually monitored by measuring temperatures at different depths in the melt, and the solidified MMCs were sectioned into disks and chemically analyzed for SiC volume fraction. The results point out that the cooling rate increased with increasing volume fraction of SiC particles. A small increase in the bulk SiC volume fraction of the cast MMC was observed due to particle settling during solidification. A one-dimensional enthalpy model of MMC solidification was formulated, wherein particle settling occurring in the solidifying matrix was coupled to the enthalpy equation by means of the Richardson–Zaki hindered settling correlation. A comparative study of simulations with experiments suggested that the thermal response of SiC particles used in this study was similar to that of single crystals, and their presence increased the effective thermal conductivity of the composite.

I. INTRODUCTION

METAL-MATRIX composites (MMCs) are a class of advanced engineering materials in which a strong ceramic reinforcement is incorporated into a metal matrix to tailor its properties for specific applications. The most commonly used reinforcements are silicon carbide, graphite, and alumina particles and fibers. An economical processing route to make silicon carbide particle-reinforced aluminum alloy MMCs has been developed by Alcan, based on the melt stirring technique for particle incorporation. This process typically involves stirring approximately 15-μm SiC particles into an aluminum-silicon alloy melt with a suitable mechanical stirrer. Following particle incorporation, the molten composite can be cast by various methods, such as investment casting and squeeze casting. Indeed, the potential for widespread use of MMCs stems from their flexibility to smoothly adapt to existing foundry practice for near-net shape casting.

The solidification process is a crucial step that largely determines the pattern of particle distribution and microstructure of the solidified MMC which, in turn, influence many of the properties of the MMC. Solidification of particle-reinforced MMCs can depend on factors solely attributable to the presence of inert ceramic particles in the melt, such as particle settling or flotation, leading to local variations of particle volume fraction and thermophysical properties of the melt, as well as interaction between the particles and solidification front. The latter is mainly determined by the solidification rate and the morphology of solidification structure and may lead to particle capture by the front in some cases and to particle pushing in others. Both settling and particle-front interaction during solidification may significantly influence the distribution pattern of the particles in the solidified MMC.

A large body of work exists on the interaction of a single inert particle with a planar solidification front and the determination of the critical front velocity above which particle capture is expected to occur. The distortion of the plane front due to thermal conductivity mismatch between the particle and melt and its implication in particle pushing have been addressed by several authors.[1–5] The morphology of the solidifying front can change in the situation where the particle ahead of the front forms a physical barrier to solute diffusion, which leads to a solute buildup behind the particle. A qualitative discussion of this phenomenon and its effect on particle pushing is offered by Sekhar and Trivedi.[6] A comprehensive summary of the preceding topics is available in a recent state-of-the-art review by Mortensen and Jin.[7] Other related studies have dealt with the mixing and settling of ceramic particles and cluster formation in molten metals[8–11] and the influence of settling and particle pushing on the microstructure and mechanical properties of MMCs.[12,13]

However, studies dealing with the heat-transfer aspects of particle-reinforced MMC solidification are notably scarce. This has left a gap in knowledge of such important areas of MMC solidification as metal-mold interfacial heat transfer and the effect of particles in the melt on its thermophysical properties, which critically influence the solidification behavior. It is the aim of the present article to address the subject of heat transfer during MMC solidification, both experimentally and by means of a mathematical model. Comparisons are made between the solidification behavior of MMCs with various volume fractions of SiC particles, up to 0.15, and that of the unreinforced alloy to reveal the effects of the particles on solidification.

G.S. HANUMANTH, Research Associate, and G.A. IRONS, Dofasco/NSERC Professor of Process Metallurgy, are with the Department of Materials Science and Engineering, McMaster University, Hamilton, ON, Canada L8S 4L7.

Manuscript submitted May 9, 1995.

II. EXPERIMENTAL

A. *Apparatus*

The silicon carbide particle-reinforced aluminum alloy MMCs were prepared by the melt stirring technique in a clay graphite crucible with an inside diameter of 0.3 m, placed inside a 10 kW resistance-heated furnace. The SiC particles were mixed into the melt using a pitched-blade turbine impeller having a diameter of 0.1 m. The impeller was fabricated from graphite and driven by a variable speed AC motor. Further details are available elsewhere.[8,9]

A schematic diagram of the instrumented mold in which unidirectional solidification of the MMC was carried out is shown in Figure 1. It consists of a split cylindrical steel mold of dimensions 40-mm i.d. and 200-mm height. Freezing took place on a solid cylindrical copper chill, 35 mm in height, which was fitted to the bottom of the mold. The thermocouples used for temperature measurement were of K type and were located at approximately 1, 50, 100, and 125 mm from the chill face. The mold was wrapped with alumina wool insulation, and the chill left exposed to convect heat to the ambient. Two additional thermocouples were used: one was used to measure the mold wall temperature, and the second was used to measure the chill temperature. All the thermocouples were interfaced to a microcomputer for data logging.

B. *Materials*

The metal matrix used in this study was a commercial foundry alloy A356 (Alcan International Ltd., Guelph, Ontario, Canada), which is often used for MMC manufacture. The major alloying elements in this alloy are 7.3 wt pct Si and 0.33 wt pct Mg. The high silicon content is known to inhibit the formation of the brittle phase Al_4C_3 at the metal-SiC interface. To promote the wetting of SiC particles, the A356 alloy was modified by adding an extra dose of Mg to increase its total content to 1.5 wt pct.

The silicon carbide particles used in the experiments were supplied by Exolon-Esk Co. (Tonawanda, NY). The size distribution of the particles was measured with a Horiba CAPA-700 Particle Analyser (Horiba Ltd., Kyoto, Japan). The particles had a median size of 15 μm and a standard deviation of 8 μm.

C. *Procedure*

1. *Solidification experiments*

The silicon carbide particle-reinforced modified A356 alloy MMCs were prepared by the melt stirring technique, as described by the authors in a previous article.[8] Briefly, about 26 kg of alloy was heated to about 700 °C in the clay graphite crucible placed inside a resistance-heated furnace. Then, the desired amount of 15-μm SiC particles was added to the modified A356 melt and mixed by means of the graphite impeller at 550 rpm for up to 3 hours to ensure that the particles were completely wetted.

The assembled mold was preheated by means of an immersion heater to a temperature of about 550 °C, while the temperatures at different locations were recorded by the computer at successive intervals of 5 seconds. After the preheating stage, a known volume of the MMC melt was transferred from the crucible into the mold with a ladle, the melt volume being chosen so as to obtain a casting approximately 150 mm in height. The melt was allowed to solidify inside the mold, and temperatures at different locations in the melt were recorded for a further duration of 3 hours. The experiment was performed for particle volume fractions of 0.0, 0.05, 0.10, and 0.15.

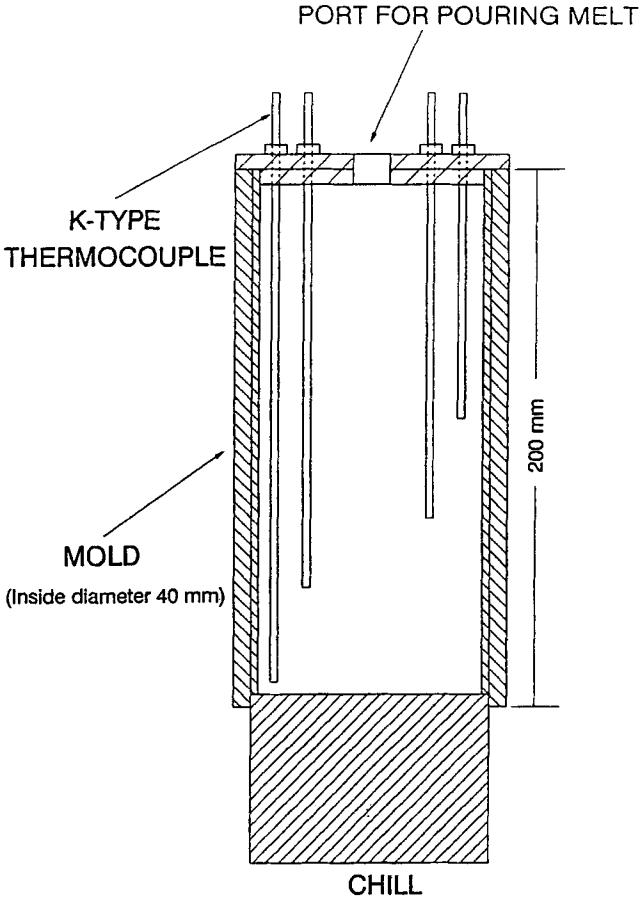

Fig. 1—The thermocouple-instrumented mold used for the unidirectional solidification experiments.

2. *Silicon carbide volume fraction measurement*

Thin sections were cut from the castings at distances of 0, 50, and 100 mm from the base and analyzed for silicon carbide volume fraction in the following manner.[8] First, the density of the sample ρ_c was determined using a standard specific gravity bottle and the Archimedes' principle. Following this, the sample was analyzed for carbon content in a LECO* Volumetric Carbon Analyzer. Knowing the carbon concentration of the sample and the stoichiometry of silicon carbide, the volume fraction of SiC, ϕ_p, is readily calculated from the expression

$$\phi_p = \left(\frac{\text{wt pct carbon}}{100}\right)\left(\frac{\text{at. wt SiC}}{\text{at. wt carbon}}\right)\left(\frac{\rho_c}{\rho_p}\right) \quad [1]$$

*LECO is a trademark of LECO Corporation, St. Joseph, MI.

III. MATHEMATICAL MODEL

A. *Model Formulation*

A one-dimensional mathematical model of MMC solidification is formulated using the enthalpy method. This

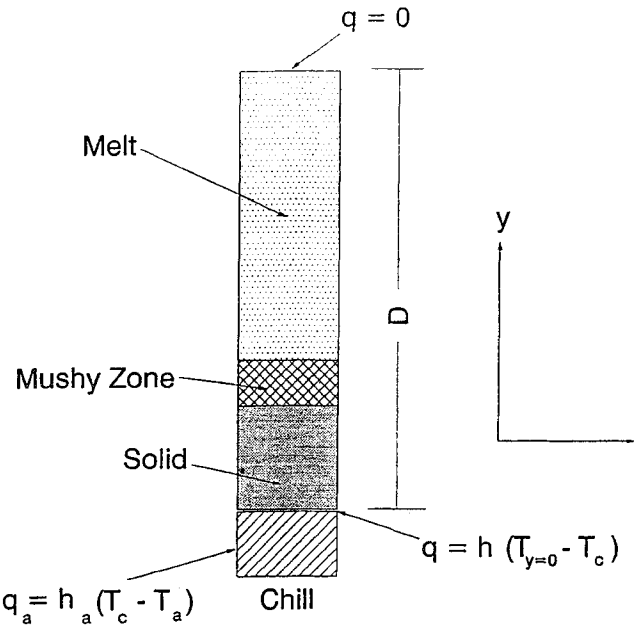

Fig. 2—A schematic illustration of the solidification model including the boundary conditions.

method eliminates the need to explicitly track the solidification front and is known to be effective for materials that solidify over a temperature range, such as metal alloys.[14] A schematic diagram of the model is illustrated in Figure 2. The following assumptions are involved in the formulation of the mathematical model.

(1) Solidification occurs unidirectionally in the upward direction, with the front advancing parallel to the horizontal chill face. In this configuration, the thermally induced density gradient is aligned with gravity, and therefore, natural convection is prevented.
(2) The thermophysical properties are independent of temperature.
(3) There is negligible volume change on solidification, and hence, no bulk motion occurs.
(4) The thermal conductivity of the MMC is taken to be equal to the volume fraction–weighted average value.
(5) The partially solidified "mushy" zone, which separates the fully solidified region from the melt, is treated as a continuum with properties equal to the volume fraction–weighted averages.
(6) Thermal equilibrium is rapidly established between the particles and the neighboring melt. This is a reasonable assumption because the computational time-step used is much larger than the time delay for the attainment of equilibrium, which is of the order of 10^{-6} seconds for the 15-μm SiC particles.
(7) Particle redistribution due to pushing by the solidification front is assumed to be negligible in the present work, since high solidification velocities are likely to minimize particle pushing. This assumption is supported by Figure 3, which shows the typical microstructures of as-cast composites from the present work. They indicate a fairly uniform distribution of particles in both low and high volume fraction specimens.
(8) Porosity is neglected in order to make the mathematical model tractable. Figure 3 indicates that the volume

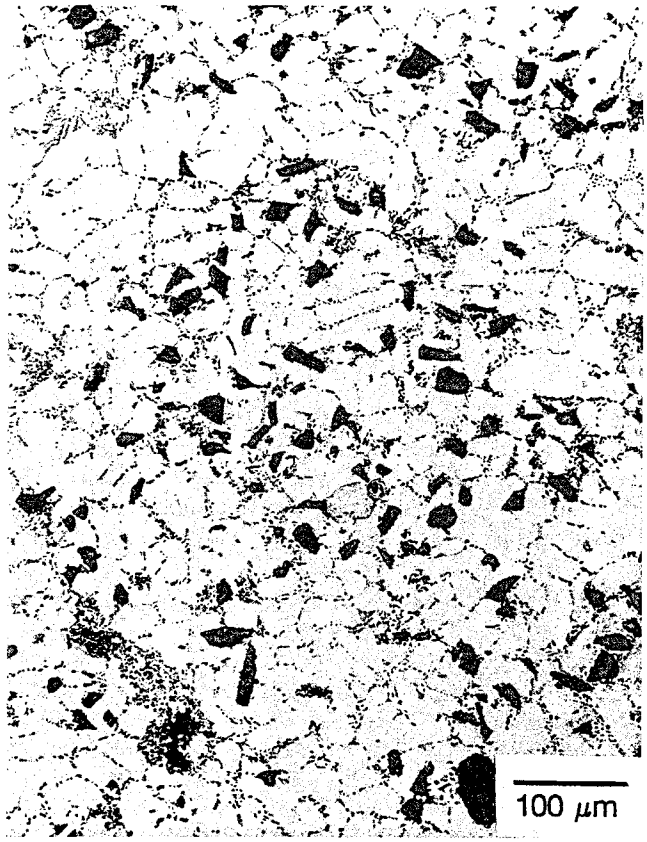

(*a*)

(*b*)

Fig. 3—Typical microstructures of as-cast modified A356 alloy MMCs reinforced with SiC particles, showing the distribution of SiC (gray angular particles) and porosity (dark regions) in the matrix: (*a*) 0.05 volume fraction SiC and (*b*) 0.15 volume fraction SiC.

fraction of porosity in the as-cast MMC samples is small. Porosity develops during particle incorporation, solidification, and the specimen preparation procedure for microstructure measurement. Measurements carried out on as-cast MMC samples of the present study indicate that porosity values range from 0.01 to 0.03 volume fraction.

With the preceding assumptions, heat balance in the melt is expressed in terms of enthalpy as

$$\frac{\delta H}{\delta t} = \frac{\delta}{\delta y}\left[K \frac{\delta T}{\delta y}\right] \quad [2]$$

The rate of change of enthalpy is the algebraic sum of contributions from transient terms, convection terms arising from particle settling and melt displacement, and the latent heat source term. Therefore, Eq. [2] may be expanded to

$$\rho_s C_s \frac{\delta}{\delta t}[\phi_s T] + \rho_L C_L \frac{\delta}{\delta t}[\phi_L T] + \rho_p C_p \frac{\delta}{\delta t}[\phi_p T] + \rho_p C_p \frac{\delta}{\delta y}[U_p \phi_p T] + \rho_L C_L \frac{\delta}{\delta y}[U_L \phi_L T] + \rho_L L\left[\frac{\delta \phi_L}{\delta t}\right] = \frac{\delta}{\delta y}\left[K \frac{\delta T}{\delta y}\right] \quad [3]$$

The following initial and boundary conditions apply.

(a) At $t = 0$, $T = T_0$ for $y \geq 0$.
(b) At $y = 0$, $q = h_c (T_{y=0} - T_{ch})$ for $t > 0$.
(c) At $y = D$, $q = 0$.

The rigorous calculation of the particle settling velocity U_p involves the solution of the coupled momentum and continuity equations.[2] However, an alternative that simplifies the computational process is to estimate the settling velocity U_p with the well-established hindered settling equation of Richardson and Zaki:[15]

$$U_p = U_0 (1-\phi_p)^{4.65} \quad [4]$$

where U_0 is the Stokes velocity for an isolated settling unit in an infinite expanse of fluid:[16]

$$U_0 = \frac{g d_p^2 \Delta\rho}{18 \mu} \quad [5]$$

Following the estimation of U_p, a simple volumetric balance yields the liquid velocity U_L. In order to sustain the solidification process until completion, the heat extracted by the chill is allowed to dissipate to the atmosphere by free convection at a rate given by the following expression:

$$q_a = h_a (T_c - T_a) \quad [6]$$

B. *Heat-Transfer Coefficients*

The model contains two heat-transfer coefficients: the first is an internal resistance between the metal and chill characterized by the contact conductance h_c, and the second is an external heat-transfer resistance represented by a heat-transfer coefficient h_a for free convection from the chill to the atmosphere.

Free convection from the chill surface lies in the laminar regime, as indicated by the Grashof number value for air, which is of the order of 10^6, well below the critical value of 10^8 for the transition to turbulent convection.[17] For free convection in the laminar regime, an appropriate relationship for the heat-transfer coefficient h_a can be expressed in terms of the Nusselt number, Nu, the Grashof number, Gr, and the Prandtl number, Pr, as follows:[17]

$$\mathrm{Nu} = 0.59 (\mathrm{Gr}\,\mathrm{Pr})^{1/4} \quad [7]$$

which, for the case of air, yields the following simplified form for the heat-transfer coefficient, h_a:

$$h_a = 1.42 (\Delta T/L)^{(1/4)} \quad [8]$$

where ΔT is the temperature difference between the chill and the ambient, and L is the chill height; the chill temperature is assumed to remain constant at its initial temperature in order to calculate ΔT.

The contact conductance, h_c, is not amenable to such a direct evaluation. It is known to be a complex function of the gap width between the chill surface and the metal, the surface roughness, the contact pressure, and the individual thermal conductivities of the metal and chill. Moreover, the gap width is likely to change with time due to the thermal expansion mismatch between the metal and chill. In this situation, it is necessary to resort to a calibration procedure to estimate the value of h_c. In this method, h_c is estimated by forcing the model to reproduce with good agreement a single set of measured melt cooling data, using h_c as a variable parameter. This is accomplished by starting with a guess value for h_c and progressively updating this value by a trial-and-error procedure until good agreement between measurement and prediction is obtained. The value of h_c thus estimated is assumed to be constant, regardless of any variation in simulation conditions, including the addition of particles to the melt.

Numerical solution

Equation [3] was discretized using the fully implicit control volume finite difference method, as described by Patankar.[18] Following the routine integration procedure, the discretized form of Eq. [3] can be expressed as

$$-a_i T(i-1,j+1) + b_i T(i,j+1) - c_i T(i+1,j+1) = d_i T(i,j) - e_i T(i+1,j) + f_i T(i-1,j) - S_i \quad [9]$$

where the coefficients are given by

$$a_i = -\frac{K_{i+\frac{1}{2}}}{\Delta y} \quad [10]$$

$$c_i = -\frac{K_{i-\frac{1}{2}}}{\Delta y} \quad [11]$$

$$b_i = \frac{\Delta y}{\Delta t}\left(\rho_s C_s \phi_s(i,j) + \rho_L C_L \phi_L(i,j) + \rho_p C_p \phi_p(i,j) + \frac{(K_{i+1/2} + K_{i-1/2})}{\Delta y}\right) \quad [12]$$

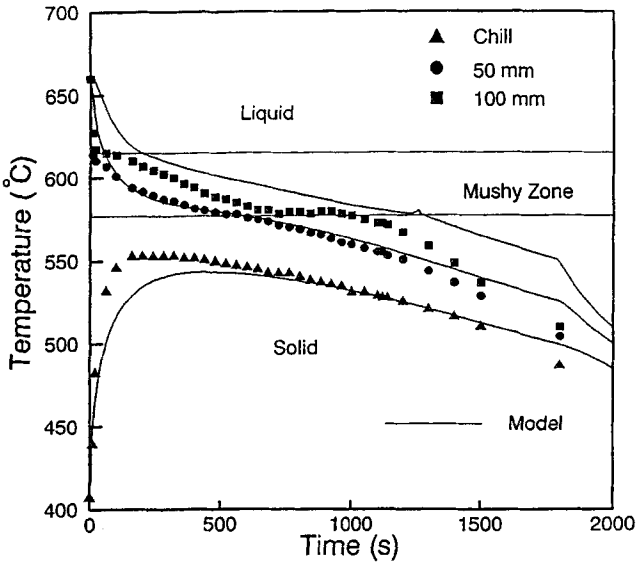

Fig. 4—Cooling curves for the solidification of unreinforced alloy.

$$d_i = \frac{\Delta y}{\Delta t}(\rho_s C_s \phi_s(i,j) + \rho_L C_L \phi_L(i,j) + \rho_p C_p \phi_p(i,j)) + \rho_p C_p (U_p(i,j) \phi_p(i,j)) - \rho_L C_L (U_L(i,j) \phi_L(i,j)) \quad [13]$$

$$e_i = \rho_p C_p (U_p(i+1,j) \phi_p(i+1,j)) \quad [14]$$

$$f_i = \rho_L C_L(U_L(i-1,j) \phi_L(i-1,j)) \quad [15]$$

$$S_i = \rho_L L \frac{\Delta y}{\Delta t}(\phi_L(i,j+1) - \phi_L(i,j)) \quad [16]$$

Because of the nonhomogeneity of MMCs, the thermal conductivity at the interface between any two control volumes is better represented by the harmonic mean value of the grid values rather than the grid values themselves or their arithmetic mean value.[18] Also, the use of harmonic mean thermal conductivity ensures heat flux consistency at the interfaces. The harmonic mean values of interface thermal conductivities are given by

$$K_{i+\frac{1}{2}} = \frac{2 K_i K_{i+1}}{K_i + K_{i+1}} \quad [17]$$

$$K_{i-\frac{1}{2}} = \frac{2 K_{i-1} K_i}{K_{i-1} + K_i} \quad [18]$$

The discretization Eq. [12] forms a tridiagonal matrix for the grid points $i = 1$ to n. The tridiagonal matrix of algebraic equations was solved using the Thomas algorithm.[19] The grid spacing and the time-step used were 1 mm and 0.05 seconds, respectively.

The nonlinear latent heat source term was handled by iteration as follows. A liquid volume fraction (ϕ_L) field was assumed for the mushy zone where latent heat is released during solidification, which enabled computation of the temperature field using the mathematical model. The validity of the assumed liquid fractions was ascertained by using the Scheil Eq. [20] for each grid point located in the mushy zone. Accordingly, the computed temperature field, corresponding to the assumed liquid volume fractions, was compared with the temperatures calculated from the Scheil equation:

$$T = T_f - (T_f - T_L) \phi_L^{k-1} \quad [19]$$

where k is the partition coefficient equal to 0.117 for Al-Si alloy.[21] If the temperatures did not agree, a correction was applied to the liquid fractions and the computation repeated. For liquid fractions above the eutectic temperature (577 °C), the correction was of the form

$$\phi_L^c = \phi_L^p + \lambda(\phi_L - \phi_L^p) \quad [20]$$

where

$$\phi_L = \left(\frac{T_f - T}{T_f - T_L}\right)^{-\frac{1}{k-1}} \quad [21]$$

and T is the computed grid temperature of a mushy control volume. The term λ is an under-relaxation factor whose value is 0.1. If at any time-step a control volume attained the eutectic temperature (577 °C), then it was constrained to isothermally release its remaining latent heat. In this manner, the solution was iterated until the calculated and Scheil temperatures converged to within 0.5 °C.

At the completion of a time-step, the volume fractions and the chill temperature (T_{ch}) were updated, and the computation process repeated for a total time of 2000 seconds. The particle volume fraction ϕ_p was updated by adding to the existing value the amount of particles which accumulated by settling over a given time-step, whereas the computed liquid fractions were retained as starting values for the following time-step. Particle settling was switched off locally if during the computations a control volume attained a close-packed structure, that is, when the combined volume fraction of the solidified matrix and particle became 0.6.

At the end of each time-step, the chill temperature (T_{ch}) was updated by adding the net heat extracted from the metal as follows:

$$T_{ch}^c = T_{ch}^p + \frac{(q - q_a)\Delta t}{W_{ch} C_{ch}} \quad [22]$$

where the superscripts c and p refer to the current and previous values of the variable, q is the quantity of heat flowing across the metal-chill interface, q_a is the convective heat flow to the atmosphere, and W_{ch} and C_{ch} are the weight and specific heat of the chill, respectively.

IV. RESULTS

A. *Cooling Rates*

Figure 4 shows the results of the solidification experiment for the unreinforced alloy. The thermophysical properties used in the computations are listed in Table I. The predictions shown in Figure 4 are based on a value of the interfacial conductance h_c equal to 48 kW m^{-2} K^{-1}.

Using the solidification model and the previous value of h_c, computations were carried out for two different values of SiC thermal conductivity and a range of volume frac-

Table I. Thermophysical Properties of the Materials

Property	Solid	Liquid	SiC
Density (ρ) (kg m^{-3})	2700[28]	2400[28]	3200[29]
Specific heat (C_p) (J kg^{-1} K^{-1})	1084[29]	963[28]	1300[30]
Thermal conductivity (K) (W m^{-1} K^{-1})	159[28]	121[29]	100[22]
Latent heat (L) (kJ kg^{-1})	—	389[28]	—
Viscosity (μ) (kg m^{-1} s^{-1})	—	0.002[3]	—
Liquidus temperature (T_L) (°C)	—	615[31]	—
Solidus temperature (T_s) (°C)	—	577[31]	—
Melting point of aluminum (T_f) (°C)	—	660[29]	—
Chill (copper) density (ρ_{ch}) (kg m^{-3})	8900[28]	—	—
Chill (copper) specific heat (C_{pch}) (J kg^{-1} K^{-1})	385[28]	—	—

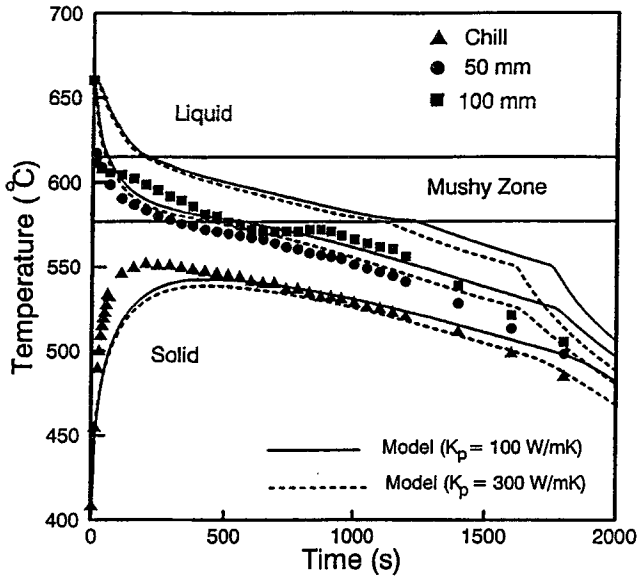

Fig. 5—Cooling curves for the 0.05 volume fraction SiC particle-reinforced MMC.

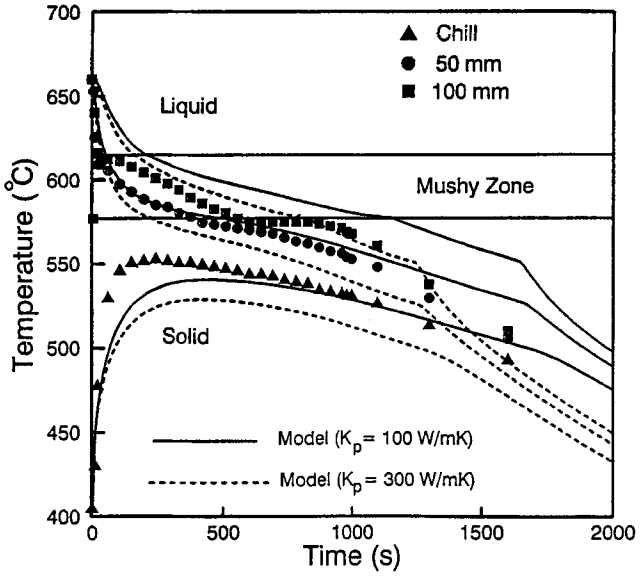

Fig. 6—Cooling curves for the 0.15 volume fraction SiC particle-reinforced MMC.

tions. For the first set of computations, the thermal conductivity was chosen to be 100 W m^{-1} K^{-1} based on measurements reported by Zweben[22] for similar MMCs. In

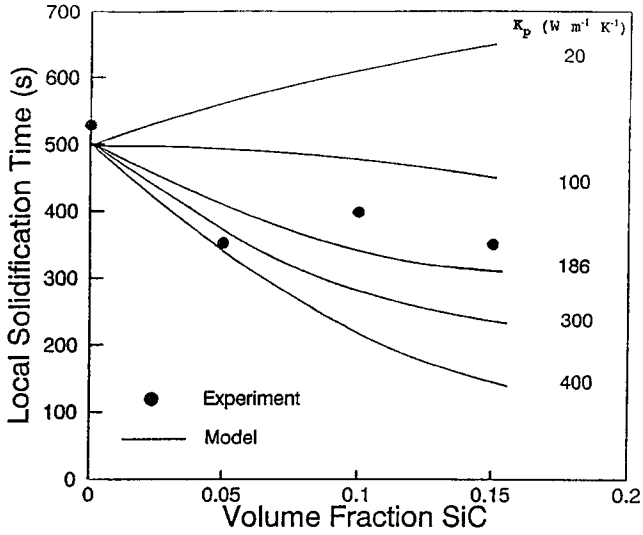

Fig. 7—The dependence of local solidification time on SiC volume fraction with SiC thermal conductivity as a parameter.

the second set of computations, the SiC thermal conductivity value was set to 300 W m^{-1} K^{-1}, which corresponds to the value for a single crystal structure. The issue of the particle thermal conductivity is addressed in Section V.

A general examination of the results shows that they conform to the expected stagewise cooling behavior: a rapid dissipation of superheat followed by a deceleration of cooling rate in the mushy zone due to latent heat release, and an accelerated cooling rate when solidification is complete and latent heat exhausted. An extended eutectic solidification region is evident at the height of 100 mm as compared to 50 mm, whereas the eutectic region predicted by the model appears to be shorter, which might indicate that the latent heat release in the mush may have a different dependence on mush temperature than the Scheil relationship (Eq. [19]) employed in the present study. Good agreement is noted between prediction and experiment for the 50-mm height, but the model underestimates the cooling rate at the higher location of 100 mm. The deviation between experiment and model appears to increase in the postsolidification cooling stage.

The results for the MMCs with 0.05 and 0.15 volume fraction SiC are shown in Figures 5 and 6. While the broad trends appear to remain unchanged from the unreinforced alloy, a close examination of the results reveals an increase in the cooling rate for the MMCs relative to the unreinforced alloy. The increase of cooling rates in the presence of

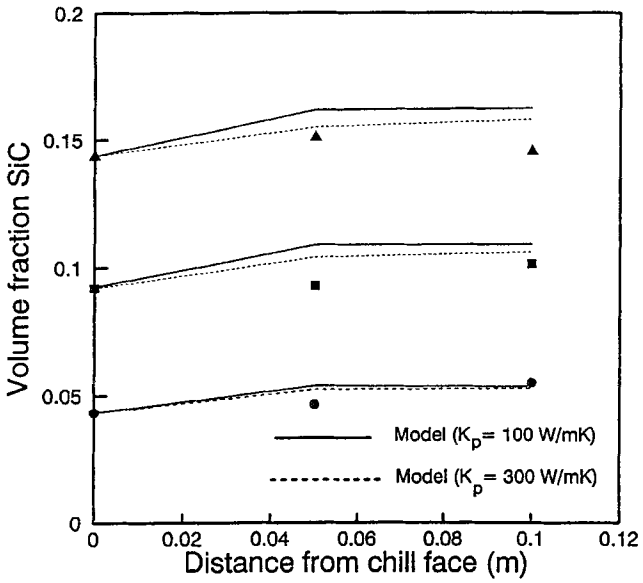

Fig. 8—Silicon carbide volume fraction profiles for MMCs cast from melts with different initial SiC volume fractions.

silicon carbide particles can be readily noticed in Figure 7, wherein the local solidification time at a distance of 50 mm from the base is plotted as a function of initial silicon carbide volume fraction in the melt, with SiC thermal conductivity as a parameter. The local solidification time is defined as the time interval in which the melt cools down from the liquidus temperature (615 °C) to the solidus temperature (577 °C). The measured local solidification time indicates a large drop in its value upon adding 5 vol pct SiC to the melt and little change with further additions of SiC. On the other hand, local solidification times predicted by the model are considerably higher than the experimental values at all volume fractions when SiC thermal conductivity is lower than 100 W m^{-1} K^{-1}.

B. *Particle Settling*

Figure 8 shows the SiC volume fraction as a function of distance from the base for initial melt nominal volume fractions of 0.05, 0.1, and 0.15. The experimental results indicate a slight increase in volume fraction of SiC with distance from the base in the 5 and 10 pct MMCs, whereas in the 15 pct case, a slight increase occurs only at the 50-mm distance. In contrast, the model predicts a much larger increase in volume fractions for all MMCs at the distance of 50 mm, but there is hardly any further increase at 100-mm distance. As in the case of cooling rates, the predictions match experiments more closely when SiC thermal conductivity is chosen to be 300 W m^{-1} K^{-1}.

V. DISCUSSION

A. *Cooling Rates*

The observed increase in cooling rate upon addition of SiC particles cannot be fully accounted for by the accompanying decrease in latent heat content of the melts. For instance, 0.15 volume fraction SiC decreases the latent heat content by 15 pct, whereas calculation using the value of 100 W m^{-1} K^{-1} for SiC thermal conductivity and the rule-of-mixtures for the effective thermal conductivity shows that the thermal diffusivity of the melt decreases by about 10 pct as a result of particle addition. Thus, the benefit gained by a reduction in latent heat content is largely offset by the decrease in thermal diffusivity, and cooling rates are expected to change only marginally in the presence of SiC particles, as indeed the predicted results of Figure 7 demonstrate.

By contrast, the experimental results indicate that local solidification times decrease by as much as 25 to 30 pct as the volume fraction changes from 0 to 0.15. A possible explanation for this observation could be that the effective thermal conductivity of the melt increases upon adding SiC particles to it. Because the density and specific heat of the alloy and SiC are also different, the thermal diffusivity is more appropriate for comparison. The thermal diffusivity of the composite melt based on the rule-of-mixtures may be expressed as

$$\alpha_c = \frac{\phi_p K_p + (1-\phi_p) K_m}{(\phi_p \rho_p + (1-\phi_p) \rho_m)(\phi_p C_{pp} + (1-\phi_p) C_{pm})} \quad [23]$$

By setting Eq. [23] equal to the matrix thermal diffusivity, it is possible to calculate a critical value for SiC thermal conductivity, a value above which SiC will increase the effective thermal diffusivity of the composite to a value higher than that of the matrix. If the SiC thermal conductivity is equal to or lower than the critical value, then the melt thermal diffusivity remains unchanged or decreases upon introducing the particles, respectively. For example, in the case of 0.15 volume fraction composite, a calculation using the properties listed in Table I yields a critical thermal conductivity of 186 W m^{-1} K^{-1} for SiC. This is significantly higher than 100 W m^{-1} K^{-1}. Indeed, there are studies showing that the thermal conductivity of SiC can vary over a range of values depending on its purity and microstructure; values at room temperature of about 100 W m^{-1} K^{-1} for polycrystals and 270 to 390 W m^{-1} K^{-1} for single crystals have been reported.[23,24] Actual measurements carried out on DURALCAN* MMC samples have yielded thermal conductivity values which are higher than that of the melt;[25,26] for example, an A356 alloy with 0.15 volume fraction SiC has a conductivity of 180 W m^{-1} K^{-1} for which the effective SiC thermal conductivity is 300 W m^{-1} K^{-1}. It may be that small silicon carbide particles behave as single crystals.

*DURALCAN is a trademark of Alcan International Ltd., Guelph, Ontario, Canada.

Computations carried out using the higher value of SiC thermal conductivity (300 W m^{-1} K^{-1}) with the remaining properties unchanged are shown as broken curves in the preceding diagrams and yielded cooling curves that are in closer agreement with experiments (Figures 5 and 6). The vastly improved predictions become evident from the results of local solidification time presented in Figure 8. What is significant about these results is that the local solidification time predicted by the model undergoes a reversal of behavior depending on the value chosen for SiC thermal conductivity. This reversal appears to occur at a SiC thermal conductivity of 100 W m^{-1} K^{-1}, a value which is lower than the critical thermal conductivity of 186 W m^{-1} K^{-1}

discussed previously. This is to be expected because the addition of a given volume fraction of SiC particles to the melt results in an equivalent decrease in the amount of latent heat to be extracted during solidification.

The level of purity of the added SiC thus appears to significantly influence the solidification rate of MMCs. For instance, addition of low purity SiC with a thermal conductivity of about 20 W m^{-1} K^{-1} results in an increase in local solidification times, whereas thermal conductivity values approaching that of a single crystal result in an opposite behavior, with local solidification times decreasing with SiC. Therefore, it is important to note that for MMCs reinforced with fine SiC particles, thermal conductivity values close to the single crystal value are more appropriate than low purity values of 20 to 100 W m^{-1} K^{-1}.

B. *Particle Settling*

The experimental results (Figure 8) demonstrate that the there is only a small change in SiC volume fraction in the bulk of the solidified casting. In relation to experiments, the model overestimates the amount of SiC settling in the solidifying matrix, as indicated by the noticeable increase in volume fraction, particularly in the region close to the chill.

In a solidifying matrix, the properties of the matrix, such as viscosity and density, are expected to continuously change. As the melt cools, its viscosity is known to increase noticeably[27] and its density to increase slightly. Both these effects tend to reduce the particle settling rate compared to an isothermal melt bath. Furthermore, additional hindrance of settling may be offered by the crystals that are continuously precipitating in the solidifying matrix. In fact, the model demonstrates that under the experimental conditions chosen in this study, the entire melt transforms into solid and mush within about 300 seconds of solidification. This rapid transformation of the melt can indeed suppress the amount of settling that can occur in the melt as compared to settling in the absence of solidification.

The changing physical composition of the matrix and its properties are not adequately addressed in the settling model. For instance, the model assumes a constant viscosity and neglects the additional hindrance offered by the precipitating crystals in the melt; the Richardson–Zaki equation takes into account only the influence of neighboring SiC particles but not that of precipitating matrix crystals. In the neighborhood of the chill, solidification is most rapid, settling is minimal, and the original particle volume fraction is preserved, whereas far from the chill, prolonged settling gives rise to a higher particle volume fraction until the entire melt becomes saturated with crystals and particles and settling practically comes to a halt.

VI. CONCLUSIONS

The following conclusions can be drawn from the study.

1. The cooling rate of modified aluminum A356 alloy melts increases with the addition of 10- to 15-μm silicon carbide particles.
2. A one-dimensional enthalpy model for MMC solidification, which incorporates the particle settling occurring in the solidifying matrix, was formulated and shown to provide good agreement with cooling rates and macroscopic particle redistribution in the melt.
3. For accurate representation of cooling rates and macroscopic particle redistribution due to settling, the silicon carbide particle thermal conductivity must be 200 to 400 W m^{-1} K^{-1}, approaching values for single crystals. Accordingly, the effective thermal conductivity of the MMC melt increases in the presence of the particles.
4. The Richardson–Zaki correlation for particle settling slightly overestimates the settling rates in the solidifying melts, possibly because it neglects the interaction between the particles and the precipitating crystals.

ACKNOWLEDGMENTS

The financial support of an NSERC/Industrial Consortium on MMCs, including Alcan International, Inco Ltd., Ontario Hydro, Sherritt Gordon Ltd., and Com Dev Ltd., is gratefully acknowledged, as is the experimental assistance of Mr. O. Kelly.

NOMENCLATURE

d	diameter (μm)
g	gravitational acceleration (m s^{-2})
h	heat-transfer coefficient (W m^{-2} K^{-1})
H	enthalpy (J)
i	space index
j	time index
k	partition coefficient
K	thermal conductivity (W m^{-1} K^{-1})
L	latent heat of fusion (J kg^{-1})
q	heat flux (W m^{-2})
t	time (s)
T	temperature (°C)
U	velocity (m s^{-1})
y	vertical coordinate (m)
Δt	time-step (s)
Δy	space-step (m)

Subscripts

a	ambient
ch	chill
l	liquid
p	particle
s	solid

Greek

α	thermal diffusivity (m^2 s^{-1})
ϕ	volume fraction
ρ	density (kg m^{-3})
μ	viscosity (kg m^{-1} s^{-1})

REFERENCES

1. P.K. Rohatgi, R. Asthana, and S. Das: *Int. Met. Rev.*, 1986, vol. 31, pp. 115-39.
2. M. Yemmou, M.A. Azouni, and P. Casses: *J. Cryst. Growth*, 1993, vol. 128, pp. 1130-36.
3. D.M. Stefanescu, B.K. Dhindaw, S.A. Kacar, and A. Moitra: *Metall. Trans. A*, 1988, vol. 19A, pp. 2847-55.
4. R. Sasikumar: *Metall. Trans. A*, 1992, vol. 23A, pp. 2326-30.
5. Y. Wu, H. Liu, and E.J. Lavernia: *Acta. Metall. Mater.*, 1994, vol. 42, pp. 825-37.

6. J.A. Sekhar and R. Trivedi: *Mater. Sci. Eng.*, 1991, vol. A147, pp. 9-21.
7. A. Mortensen and I. Jin: *Int. Mater. Rev.*, 1992, vol. 37, pp. 101-28.
8. G.S. Hanumanth and G.A. Irons: *J. Mater. Sci.*, 1993, vol. 28, pp. 2459-65.
9. G.S. Hanumanth, G.A. Irons, and S. Lafreniere: *Metall. Trans. B*, 1992, vol. 23B, pp. 753-63.
10. G.A. Irons and K. Owusu-Boahen: *Metall. Mater. Trans. B*, 1995, vol. 26B, pp. 981-89.
11. N. Setargew, B.A. Parker, and M.J. Couper: *Proc. Advanced Composites 93*, Wollongong, Australia, TMS, Warrendale, PA, 1993.
12. D.J. Lloyd: *Comp. Sci. Technol.*, 1989, vol. 35, pp. 159-79.
13. A. Labib, H. Liu, and F.H. Samuel: *Mater. Sci. Eng.*, 1993, vol. A160, pp. 81-90.
14. V.R. Voller and C.R. Swaminathan: *Metall Trans. B*, 1992, vol. 23B, pp. 651-54.
15. J.F. Richardson and W.N. Zaki: *Trans. Inst. Chem. Eng.*, 1954, vol. 32, pp. 35-53.
16. R.B. Bird, W.E. Stewart, and E.L. Lightfoot: *Transport Phenomena*, John Wiley and Sons, New York, NY, 1960, p. 60.
17. J.P. Holman: *Heat Transfer*, McGraw Hill, New York, NY, 1986.
18. S.V. Patankar: *Numerical Heat Transfer and Fluid Flow*, Hemisphere, Washington, DC, 1980.
19. B. Carnahan, H.A. Luther, and J.O. Wilkes: *Applied Numerical Methods*, John Wiley and Sons, New York, NY, 1969.
20. M.C. Flemings: *Solidification Processing*, McGraw-Hill, New York, NY, 1974.
21. I. Dustin and W. Kurz: *Z. Metallkd.*, 1986, vol. 77, pp. 265-73.
22. C. Zweben: *JOM*, 1992, vol. 44, pp. 15-23.
23. Y.S. Touloukian, R.W. Powell, C.Y. Ho, and P.G. Klemens: *Thermophysical Properties of Matter*, The TPRC Data Series, IFI/Plenum, New York, NY, 1970, vol. 2, pp. 585-87.
24. E.A. Burgeimeister, W. von Muench, and E. Pettenpaul: *J. Appl. Phys.*, 1979, vol. 50, pp. 5790-94.
25. W.R. Hoover: in *Fabrication of Particulates Reinforced Metal* Composites, J. Masounave and F.G. Hamel, eds., ASM International, Materials Park, OH, 1990, pp. 115-23.
26. D. Rose: Duralcan USA, San Diego, CA, private communication, 1994.
27. F. Ajersch and M. Mada: Internal Report, Le Centre de Developpement Technologique de L'Ecole Polytechnique, Montreal, Feb. 1989.
28. *Metals Handbook*, ASM International, Materials Park, OH, 1990, vol. 2.
29. C.J. Smithells: *Metals Reference Book*, 4th ed., Plenum Press, New York, NY, 1967.
30. R.E. Kirk and D.E. Othmer: *Encyclopedia of Chemical Technology*, 3rd ed., John Wiley and Sons, New York, NY, 1979, vol. 5.
31. *Metals Handbook*, 9th ed., ASM International, Metals Park, OH, 1988, vol. 15.